

ornl

**OAK RIDGE
NATIONAL
LABORATORY**

MARTIN MARIETTA



3 4456 0004606 4

ORNL/TM-9792

**A 3-D Analysis of Maxwell's
Equations for Cavities of
Arbitrary Shape**

J. H. Whealton
G. L. Chen
R. W. McGaffey
R. J. Raridon
E. F. Jaeger
M. A. Bell
D. J. Hoffman

OAK RIDGE NATIONAL LABORATORY

CENTRAL RESEARCH LIBRARY

CIRCULATION SECTION

4300A ROOM 117

LIBRARY LOAN COPY

DO NOT TRANSFER TO ANOTHER PERSON

If you wish someone else to see this
report, send its name with report and
the library will arrange a loan.

00 0000 1 1

OPERATED BY
MARTIN MARIETTA ENERGY SYSTEMS, INC.
FOR THE UNITED STATES
DEPARTMENT OF ENERGY

Printed in the United States of America. Available from
National Technical Information Service
U.S. Department of Commerce
5285 Port Royal Road, Springfield, Virginia 22161
NTIS price codes--Printed Copy: A03; Microfiche A01

This report was prepared as an account of work sponsored by an agency of the United States Government. Neither the United States Government nor any agency thereof, nor any of their employees, makes any warranty, express or implied, or assumes any legal liability or responsibility for the accuracy, completeness, or usefulness of any information, apparatus, product, or process disclosed, or represents that its use would not infringe privately owned rights. Reference herein to any specific commercial product, process, or service by trade name, trademark, manufacturer, or otherwise, does not necessarily constitute or imply its endorsement, recommendation, or favoring by the United States Government or any agency thereof. The views and opinions of authors expressed herein do not necessarily state or reflect those of the United States Government or any agency thereof.

Fusion Energy Division

**A 3-D ANALYSIS OF MAXWELL'S
EQUATIONS FOR CAVITIES OF
ARBITRARY SHAPE**

**J. H. Whealton
G. L. Chen
R. W. McGaffey*
R. J. Raridon*
E. F. Jaeger
M. A. Bell*
D. J. Hoffman**

***Computing and Telecommunications Division, Martin Marietta
Energy Systems, Inc.**

Date Published - March 1986

**Prepared by the
OAK RIDGE NATIONAL LABORATORY
Oak Ridge, Tennessee 37831
operated by
MARTIN MARIETTA ENERGY SYSTEMS, INC.
for the
U.S. DEPARTMENT OF ENERGY
under contract No. DE-AC05-84OR21400**



3 4456 0004606 4

CONTENTS

ABSTRACT	v
I. INTRODUCTION	1
II. WAVE EQUATIONS IN VACUUM WITH PERFECTLY CONDUCTING WALLS	3
III. DESCRIPTION OF ANALYSIS	4
A. CONVERGENCE	4
B. IMPLEMENTATION OF BOUNDARY CONDITIONS	8
C. IMPOSED CONDITIONS FOR HIGHER EIGENMODES ...	9
IV. EXAMPLES	10
V. SUMMARY	16
ACKNOWLEDGMENTS	17
REFERENCES	18

ABSTRACT

A three-dimensional analysis of cavity antennas is presented. The analysis is based on the finite difference method with a successive overrelaxation convergence scheme. This method permits the calculation of resonance frequencies and corresponding electric and magnetic fields of eigenmodes in a cavity antenna with an arbitrary shape.

I. INTRODUCTION

Cavity antennas have been used for various purposes, such as communication systems, for a long time. Recently, the usefulness of cavity antennas has aroused the interest of researchers in the plasma radio-frequency (rf) heating area, especially in the ion cyclotron resonance frequency (ICRF) range.¹ Ion cyclotron resonance heating (ICRH) has been successfully used for heating experiments in tokamaks and has been chosen to demonstrate ignition heating for first-generation tokamaks, such as the Tokamak Fusion Test Reactor (TFTR), the Joint European Torus (JET), and Doublet-III. A carefully designed and fully tested resonant cavity antenna for those tokamaks is desirable. The Radio-Frequency Test Facility (RFTF) at Oak Ridge National Laboratory (ORNL) is dedicated to this mission.

To design the cavity antenna, it is necessary to understand the characteristic properties such as resonant frequency, field components and impedance, etc. For a simple cavity, we can obtain those parameters by using the equivalent circuit method² or the variational principle method³ or even by solving Maxwell's equations with analytical methods. However, these methods are very difficult or even impossible to apply to a complicated cavity such as those that are of interest for rf heating. Hence, we need to develop a three-dimensional (3-D) analysis to obtain a numerical solution of Maxwell's equations with complicated boundary conditions.

A few 3-D algorithms⁴ have been published for solving the wave equation, but none has been developed for the purpose of plasma heating. Among the existing algorithms, Hara et al.⁴ have the most complete and powerful code. However, the accuracy becomes poor for the very complicated boundary conditions, because the mesh points are easily limited by the finite element method.

A finite difference analysis 3-D Poisson equation⁵⁻⁹ was developed by the authors for use in designing and conducting neutral beam experiments. We have extended this analysis to the 3-D wave equation. Our analysis has several basic

merits. First, a finite difference method¹⁰ is used with a successive overrelaxation (SOR) convergence scheme and a method of treating boundaries that allows the cavity to have an arbitrary shape. Second, due to the SOR scheme used, we do not need to find the inverse matrix to obtain the eigenvalue, which reduces the necessary storage requirements. Third, either Dirichlet or Neumann boundary conditions are easily considered. Hence, more mesh points can be adopted for complicated boundary data or increased accuracy. However, one of the disadvantages of SOR is the existence of convergence, and the convergence rates are strongly dependent on the chosen SOR factor. The third point implies that we can solve the wave equation in terms of H components as well as E components. Examining the Helmholtz magnetic field equation is important because it produces the lowest resonance frequency (see Sec. II), which is of considerable interest in ICRF plasma heating, where low-frequency launchers of compact dimensions are desirable.

The purpose of this paper is to demonstrate the analysis and its validity by calculating the eigenfrequencies and field components of a finite rectangular waveguide and other waveguides. The applications of this algorithm to rf heating will be given in a separate paper. The structure of the remainder of this paper is as follows. In Sec. II, we briefly describe the wave equations, boundary conditions, and possible constraining conditions. In Sec. III, we describe the subject analyses. The results for specific waveguides are presented in Sec. IV. We summarize our conclusions in Sec. V.

II. WAVE EQUATIONS IN VACUUM WITH PERFECTLY CONDUCTING WALLS

Since we consider the wave equations in vacuum, Maxwell's equations with the sinusoidal time-dependent $e^{-i\omega t}$ fields, \mathbf{E} and \mathbf{H} , are

$$\nabla \cdot \mathbf{E} = 0 , \quad (1a)$$

$$\nabla \cdot \mathbf{H} = 0 , \quad (1b)$$

$$\nabla \times \mathbf{E} = i\mu_0\omega\mathbf{H} , \quad (1c)$$

$$\nabla \times \mathbf{H} = -i\varepsilon_0\omega\mathbf{E} , \quad (1d)$$

where μ_0 and ε_0 are the permeability and dielectric constant in vacuum. By combining the two curl equations and making use of the vanishing divergences, we find that both \mathbf{E} and \mathbf{H} satisfy

$$\left(\nabla + \mu_0\varepsilon_0\omega^2 \right) \begin{Bmatrix} \mathbf{E} \\ \mathbf{H} \end{Bmatrix} = 0 . \quad (2)$$

Boundary conditions on perfectly conducting walls are

$$\mathbf{n} \cdot \mathbf{E} = 0 , \quad (3a)$$

$$\mathbf{n} \times \mathbf{H} = 0 , \quad (3b)$$

where \mathbf{n} is a unit vector outward normal to the surface of boundary, namely S . Equation (3) may be stated as follows: the boundary condition on \mathbf{E} is that E_{\parallel} vanish at the surface, and the boundary condition on \mathbf{H} is that $\partial H_{\parallel} / \partial n$ vanish at the surface, where E_{\parallel} and H_{\parallel} are the parallel components of \mathbf{E} and \mathbf{H} , respectively.

Equations (2) and (3) constitute the well-known eigenvalue problem. For the perfectly conducting cavity, all components of \mathbf{E} and \mathbf{H} are real. Equation (3) can be

solved independently for three components. Since the boundary conditions on E_{\parallel} and H_{\parallel} are different, the corresponding eigenvalues will, in general, be different. There are two distinct categories of waves: transverse magnetic (TM) wave if the boundary condition is $E_{\parallel} = 0$, and transverse electric (TE) wave if the boundary condition is $\partial H_{\parallel} / \partial n = 0$. The lowest nontrivial eigenfrequency of the TE mode is lower than that of the TM mode. For rf heating, the low-frequency, compact, high-power antenna is needed because of the typical port sizes and magnetic fields on tokamaks. From plasma diagnostic techniques, the magnetic field can be directly measured by probe, but the absolute value of the electric field cannot be. Hence, solving Eq. (2) in terms of H is more practical, though it is sometimes more difficult.

For most higher eigenfrequency modes, the eigenfunctions (E or H) are degenerate. When the eigenfunctions are degenerate, we impose conditions of constraint to remove the degeneracy. Those constraint conditions could simply use Eq. (1a) or Eq. (1b).

III. DESCRIPTION OF ANALYSIS

A. Convergence

For simplicity, we discuss our numerical method in Cartesian coordinates. Thus, Eq. (2) can be rewritten in three scalar equations for H_x , H_y , and H_z :

$$\frac{\partial^2 H_x}{\partial x^2} + \frac{\partial^2 H_x}{\partial y^2} + \frac{\partial^2 H_x}{\partial z^2} + k^2 H_x = 0 \quad , \quad (4a)$$

$$\frac{\partial^2 H_y}{\partial x^2} + \frac{\partial^2 H_y}{\partial y^2} + \frac{\partial^2 H_y}{\partial z^2} + k^2 H_y = 0 \quad , \quad (4b)$$

$$\frac{\partial^2 H_z}{\partial x^2} + \frac{\partial^2 H_z}{\partial y^2} + \frac{\partial^2 H_z}{\partial z^2} + k^2 H_z = 0 \quad (4c)$$

where $k^2 = \mu_0 \epsilon_0 \omega^2$. Similar equations can be obtained for E if we replace H by E in Eq. (4).

Equation (4) is similar to the Poisson equation with a linearized source term. We have modified the validated analysis described in Ref. 6, which describes some of the details of the present analysis. In the subject analysis, we expand the fields (E or H) and their particle derivatives in Eq. (4) at node 0 (see Fig. 1) in terms of the fields

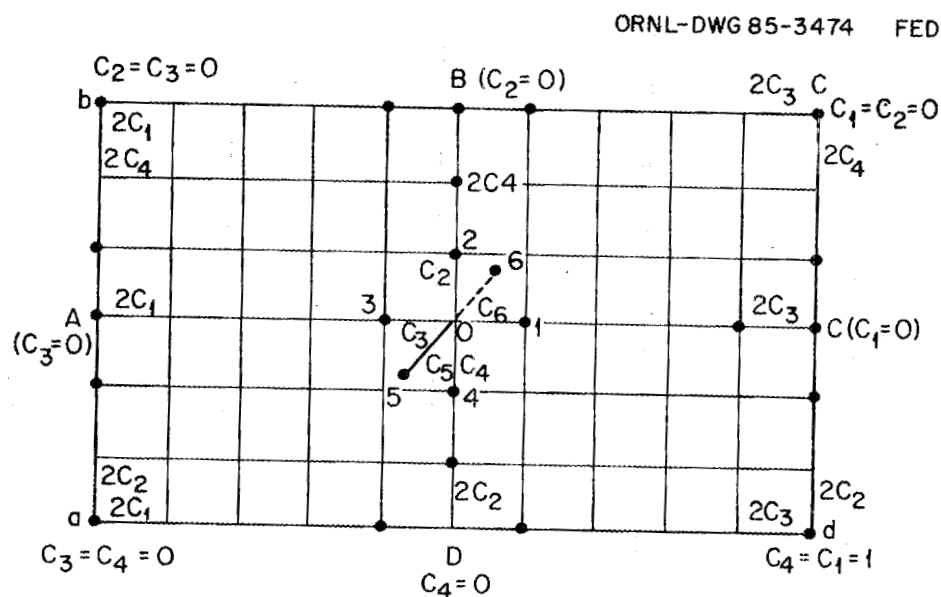


FIG. 1. The setup of nodal points and their finite difference expansion coefficients.

at its neighbor grid points (1-6) by using the first-order finite difference approximation. We have, for example,

$$\begin{aligned} H_{z0} &= C_1 H_{z1} + C_2 H_{z2} + C_3 H_{z3} + C_4 H_{z4} + C_5 H_{z5} + C_6 H_{z6} \\ &= \sum_{i=1}^6 C_i H_{zi}, \end{aligned} \quad (5)$$

where H_{zi} is the value of H_z at the i th node and C_i is the expansion coefficient in that direction.

Then, we iterate the calculation by SOR until the difference between the two sides of Eq. (5) vanishes. That is, $\text{Res} = H_{z0} - \sum_i C_i H_{zi} \approx 0$. We define this as a minor iteration. During the minor iteration, k^2 is kept constant. Once H_j (or E_j) is found, after a completed minor iteration, a new value of k^2 can be gotten from

$$k^2 = \left[\frac{+\nabla^2 H_j(\mu_{\ell m})}{H_j(\mu_{\ell m})} \right] \text{ or } \left[\frac{+\nabla^2 E_j(\mu_{\ell m})}{E_j(\mu_{\ell m})} \right], \quad (6)$$

where $\mu_{\ell m}$ is an arbitrarily chosen grid point and $H_j = H_j/H_{j \max}$. $H_{j \max}$ is the maximum value of all H_j . This new k^2 is input into a minor iteration. A major iteration is then finished. The iteration process is completed and the eigenfrequency is found when the previous k^2 and the latest k^2 are sufficiently close. An alternative way to find the new k^2 needs to be mentioned here, because it converges rapidly in most cases. We can obtain the new k^2 by dividing k^2 by $H_{j \max}$ (or $E_{j \max}$). Convergence is achieved when $H_{j \max}$ is unity. Mathematically, this corresponds to choosing the $H_j(\mu_{\ell m})$ equal to $H_{j \max}$ in Eq. (6). However, this method fails if the maximum value of H_j is assigned as a constant boundary value where the nodes are excluded from the iteration. The algorithm is shown in Fig. 2.

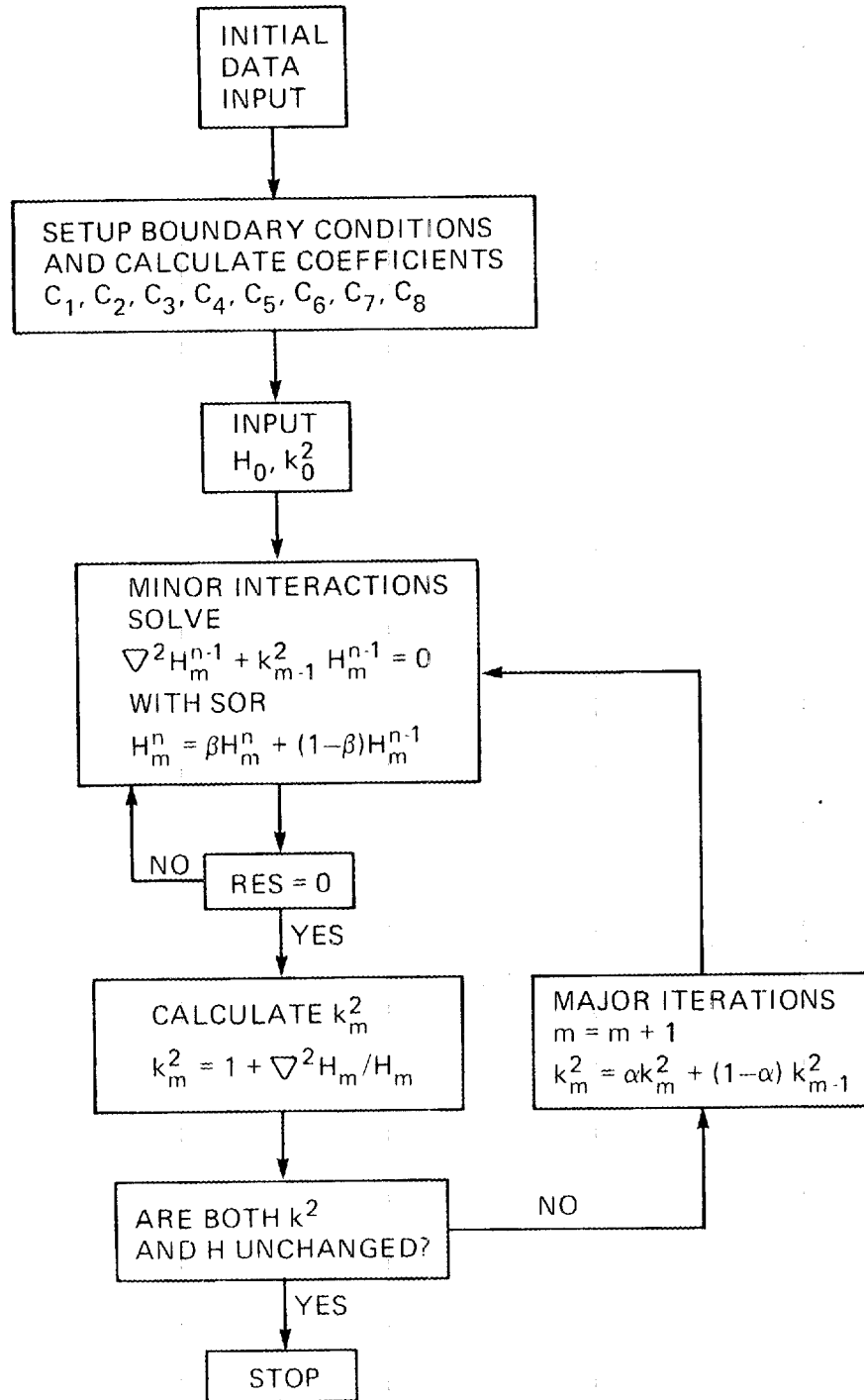


FIG. 2. Algorithm for Maxwell's equations.

Convergence is critically dependent on the relaxation parameters¹¹ for the SOR method. In the major iteration, we use underrelaxation to get the new k^2 of the m th iteration; that is,

$$k_m^2 = \alpha k_m^2 + (1 - \alpha) k_{m-1}^2, \quad (7)$$

where k_m^2 is evaluated from Eq. (6). The underrelaxation parameter, α , is in the range of $0 < \alpha \leq 1$. Similarly, we use overrelaxation with the relaxation parameter, $1 \leq \beta < 2$, in the minor iteration; that is,

$$H_j^n = \beta H_j^n + (1 - \beta) H_j^{n-1}, \quad (8)$$

where H_j^n is the result from Eq. (5). Whether or not the iteration process converges at all and whether the convergence is fast or slow depends on the chosen values of α and β . We give a more detailed discussion in Sec. IV. Theorems on the choice of α and β are being developed.

B. Implementation of Boundary Conditions

Two types of boundary conditions, either the Dirichlet boundary condition ($E_j = 0$ or $H_j = 0$) or the Neumann boundary condition ($\partial E_j / \partial x_k = 0$ or $\partial H_j / \partial x_k = 0$), are required to solve Eq. (4). For example, to solve Eq. (4c), we let $H_z = 0$ on boundary surfaces xy , $\partial H_z / \partial x = 0$ on boundary surfaces yz , and $\partial H_z / \partial y = 0$ on boundary surfaces zx , as illustrated in Fig. 3. Setting up the Dirichlet boundary condition is rather simple. We let the fields equal zero only at the nodes and keep them constant on each iteration. To treat the Neumann boundary condition, we need to redefine the coefficients C_i . For a point that lies on the boundary line, C_i is set at zero for the direction that points outside the boundary, and the opposite C_i is doubled. For

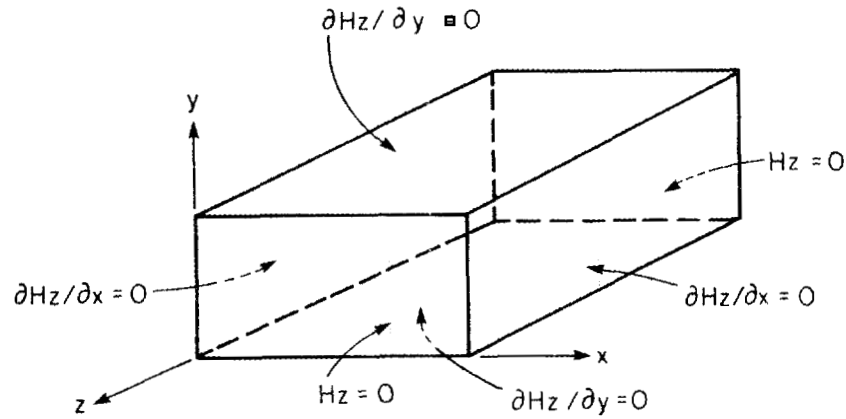


FIG. 3. Schematic representation of the cavity resonator and the boundary conditions of H_z .

example, for point A, we let $C_3 = 0$ and double C_1 ; for point B, we let $C_2 = 0$ and double C_4 ; for point C, we let $C_1 = 0$ and double C_3 , and for point D, we let $C_4 = 0$ and double C_2 . For points that lie on the corners, we double the two nonzero C_i 's that lie interior to the boundary. For example for point a, we let $C_3 = C_4 = 0$ and double C_1 and C_2 . The C_i 's for points b, c, and d need similar treatment.

We cannot expect all the boundaries to be fitted in the nodal lines. A typical case is shown in Fig. 4, a circle. This problem causes slight complications in the Neumann boundary conditions. However, here we have developed a new scheme¹² to deal with these oblique Neumann boundary conditions.

C. Imposed Conditions for Higher Eigenmodes

The procedure described above (Sec. III.A) can only produce the lowest mode, because Eq. (6) provides a bound only for the lowest eigenfrequency. To get the

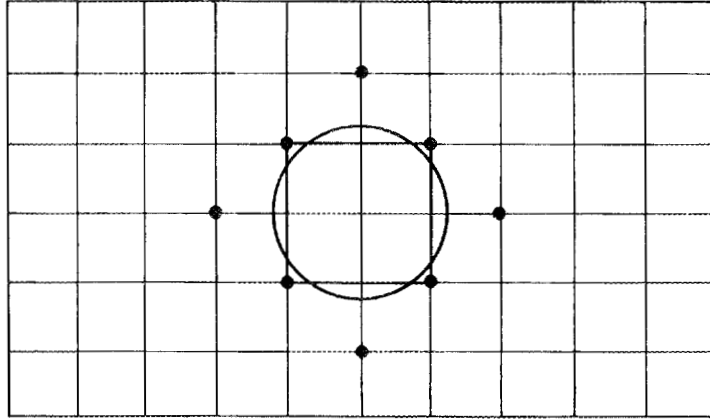


FIG. 4. A typical irregular boundary.

higher modes, we must implement the Gram-Schmidt orthogonalization. It is worth pointing out here that the lowest eigenfrequency of the TE mode is zero, and the corresponding eigenfunction is an arbitrary constant. For this particular case, we can simply obtain the first nontrivial eigenfrequency by subtracting a constant from H_j (or E_j). This constant could be the averaged value of H_j (or E_j) at each iteration. If the higher modes have degeneracy, the constraint condition $\nabla \cdot \mathbf{H} = 0$ (or $\nabla \cdot \mathbf{E} = 0$) is also required in order to exclude the undesired mode.

IV. EXAMPLES

We use a rectangular cavity, a ridged waveguide, and a complicated cavity to examine the validity of our analysis. It is well known that if a , b , and c are the dimensions of the rectangular cavity (Fig. 5a) and $c \geq a > b$, then the magnetic field and electric field of the TE_{01} mode (the lowest nontrivial mode) are

$$H_x = A \sin \frac{\pi x}{a} \cos \frac{\pi z}{c}, \quad (9)$$

ORNL-DWG 85-3478 FED

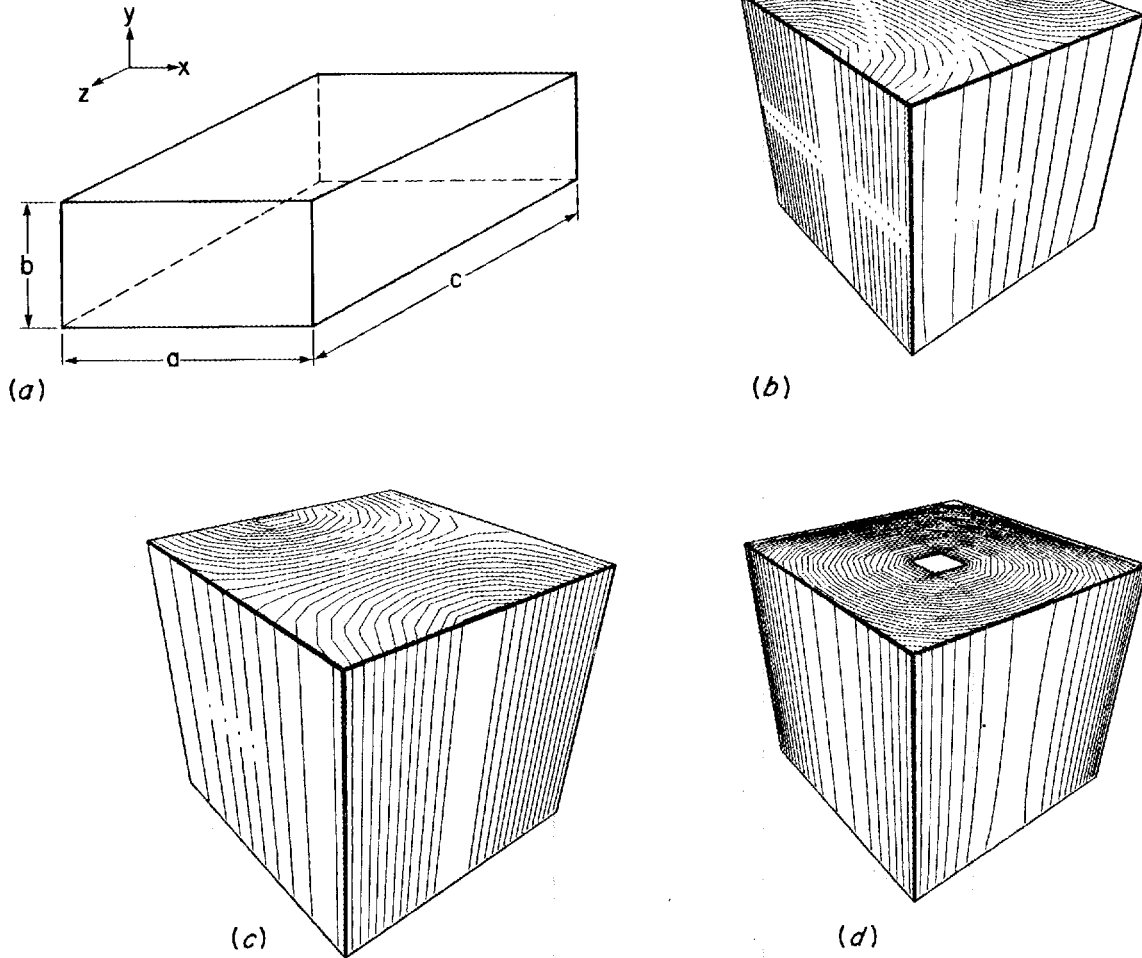


FIG. 5. Sample results for a resonant cavity: (a) the dimensions of the cavity, (b) H_z of TE_{01} wave, (c) H_x of TE_{01} wave, and (d) E_y of TE_{01} wave. The chained lines represent the negative fields, and the vector of field points to the inside of the paper.

$$H_z = B \cos \frac{\pi x}{a} \sin \frac{\pi z}{c}, \quad (10)$$

$$E_y = C \sin \frac{\pi x}{a} \sin \frac{\pi z}{c}, \quad (11)$$

$$H_y = E_x = E_z = 0, \quad (12)$$

where A, B, and C are constants.

The corresponding eigenfunction is

$$k^2 = \frac{\pi^2}{a^2} + \frac{\pi^2}{c^2}. \quad (13)$$

Figure 5 gives the results of our calculation with $a = c = 2$ m and $b = 1$ m. In this paper, the contours of the field are plotted for all examples. The difference between the value of k^2 from the subject analysis ($= 4.89 \text{ m}^{-2}$) and that from Eq. (13) ($= \pi^2/2 \text{ m}^{-2}$) is less than 1%. Since the analysis of Sec. III considers arbitrary boundary data, and since the analysis cannot determine that the example of a shoebox cavity is solvable exactly, the agreement in the lowest eigenvalue constitutes a nontrivial validation of the subject analysis.

The second example considered is that of a ridged waveguide. This waveguide has a lower cutoff frequency and a wider band of useful frequencies than a rectangular waveguide with equivalent outside dimensions. Figure 6 shows a typical ridged waveguide and its lowest mode (TE_{01}) H_z field. Figure 6(b) shows the result for an infinitely long waveguide. Infinite length is a necessary assumption for the equivalent circuit approximation.² To compare our results with the equivalent circuit approximation, the lowest eigenfrequencies of three ridged waveguides with different aspect ratios are computed by both methods. The results are plotted in Fig. 7 with apparent agreement. In order to illustrate our 3-D analysis of the finite

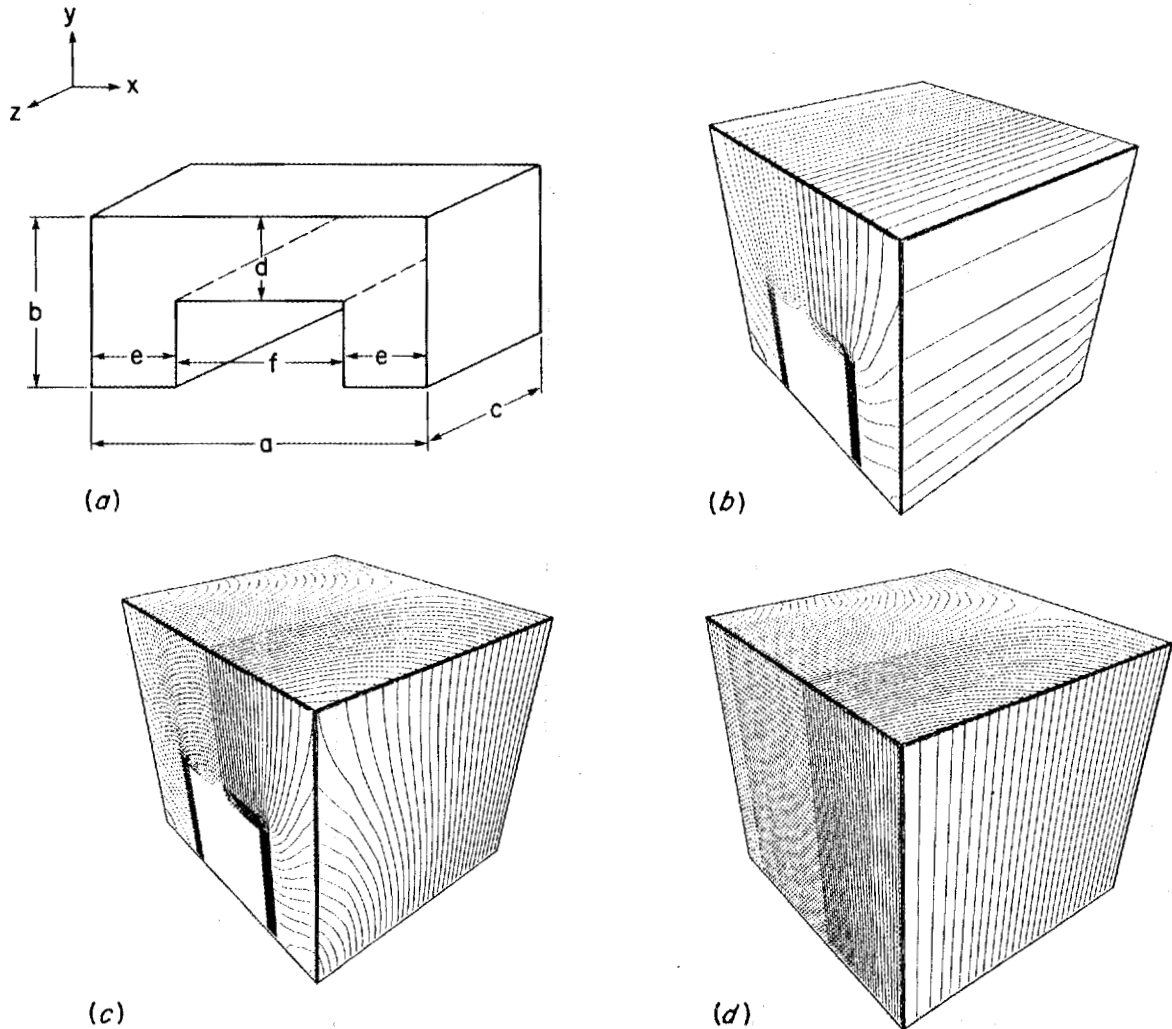


FIG. 6. Sample results for a ridged waveguide: (a) the dimensions of waveguide ($a:b:d:e = 4:2:1:1$), (b) H_z of TE_{01} wave for $c = \infty$ with both ends open, and (c) H_z of TE_{01} wave for $c/b = 1$ with closed back end. For comparison we also show (d) H_z of TE_{01} wave for a rectangular waveguide with closed back end. The dashed lines represent the negative fields and the vector of field points to the outside of the paper.

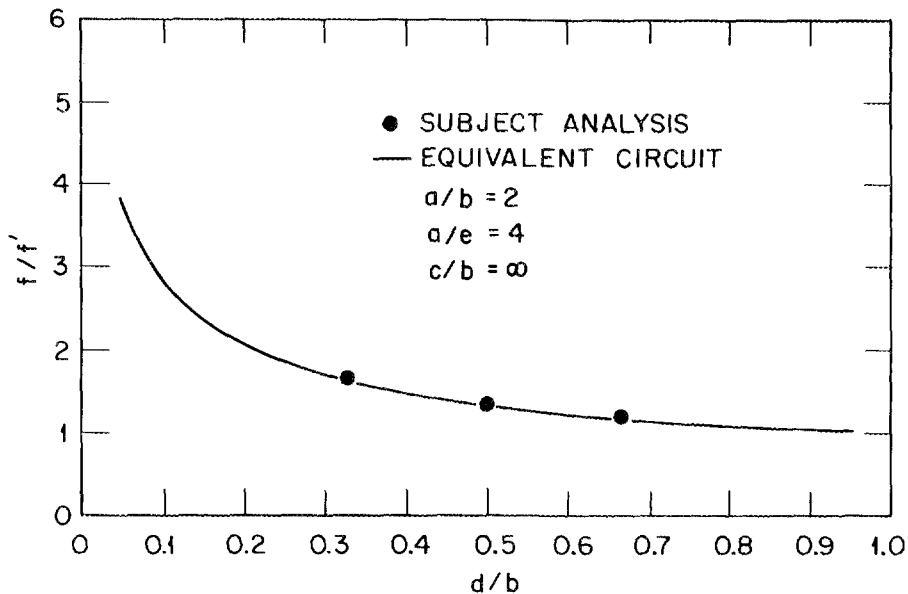


FIG. 7. Comparison of the eigenmode resonance frequencies computed with our method and with the equivalent circuit approximation by Pyle.² f/f' is the ratio of resonance frequency with the rectangular waveguide to that with the ridge.

waveguide, Fig. 6(c) shows the results for a finite ridged waveguide ($c = b$), and Fig. 6(d) shows the results for a rectangular waveguide without the ridge. Both waveguides are closed by a metallic wall at the back end. The resonance frequency for the finite-length waveguide is reduced by only 13% due to the ridged effect. From Fig. 7, we find that the resonance frequency reduction is 28% for the corresponding infinitely long waveguides.

We also use this example to discuss the correlation of convergence and the relaxation parameters, α and β . For this purpose, two ridged waveguides with different aspect ratios (one infinitely long and the other with a finite length) have

been used to study the convergence. The parameters for convergence are illustrated in Table I. For the infinitely long ridged waveguide, the result shows that convergence is speeded up with the larger α and β , if we keep the other parameters constant. In the case of the finite-length waveguide, closed only at one end with a Neumann boundary condition at the other end, the result shows that the code converges only at a particular parameter range. If the finite-length ridged waveguide is closed on both ends, then convergence is readily achieved for $0.05 < \beta \leq 1.7, 0.05 < \alpha \leq 1$.

The last example of the analysis considered here is the cavity illustrated in Fig. 8. This cavity is similar to the cavity antenna that has been proposed for the ICRH experiment in Doublet III-D. Experiments on it are proceeding at the RFTF. We have used this example to examine the consistency of our results for two different orientations. The eigenfrequencies of both cases are identical to within 3%. The

Table I. The parameters for convergence for a ridged waveguide^a

Aspect ratio	Minor iteration	β	α	Major iteration
$a = 2, b = 1, c = \infty$	45	1.0	1.0	64
			0.9	63
			0.8	72
			0.5	>100
	15	1.0	0.8	>100
			1.2	>100
			1.5	69
		1.7	34	
$a = 2, b = 1, c = 1$ (one end closed)	15	1.0	1.0	120
			0.7	80
			0.5	>120

^aThe number of nodes used here is $20 \times 18 \times 10$.

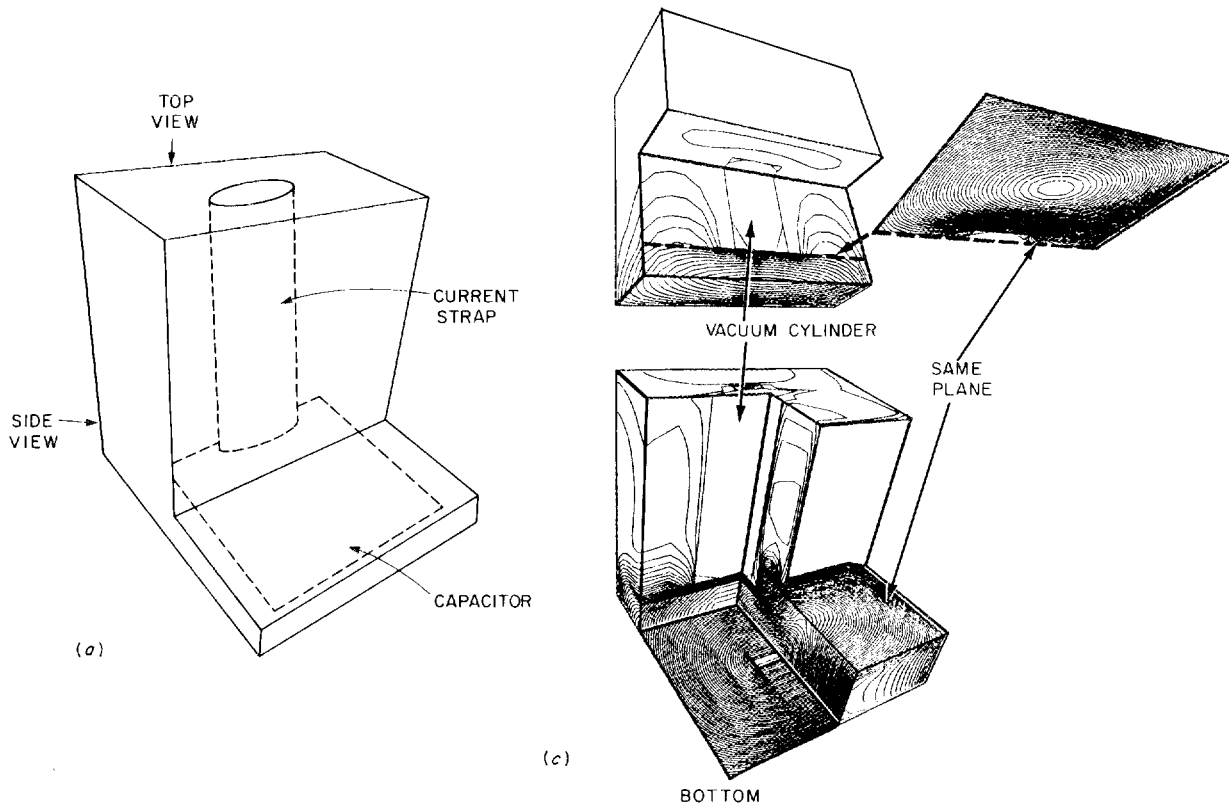


FIG. 8. Sample results for a complicated cavity: (a) structure of the cavity, (b) top view of $|E|$ field, and (c) side view of $|E|$ field.

corresponding electric fields, which are consistent in both cases, are shown in Fig. 8. This result proves that the subject analysis is independent of boundary data orientation.

V. SUMMARY

We have developed a 3-D analysis that can deduce the resonance frequencies and the wave fields for a cavity antenna of arbitrary shape by using the finite difference method with an SOR convergent scheme. This analysis has been very

carefully tested for various cavities. The results shown are in good agreement with other theoretical analyses.

ACKNOWLEDGMENTS

The authors wish to express their gratitude to D. H. Wooten for providing the interface between the subject analysis and the plotting routine, DISSPLA.

This research was sponsored by the Office of Fusion Energy, U.S. Department of Energy, under Contract No. DE-AC05-84OR21400 with Martin Marietta Energy Systems, Inc.

REFERENCES

- ¹For example, F. W. Perkins and R. F. Kluge, *IEEE Trans. Plasma Sci.* PS-12(2), 161-172 (1984).
- ²J. R. Pyle, *IEEE Trans. Microwave Theory Tech.* MTT-14 (4), 175-183 (1966); S. B. Cohn, *Proc. IRE* 35, 783-788 (1948).
- ³For example, J. Schwinger and D. S. Saxon, Discontinuities in Waveguides (Gordon and Breach, New York, 1968).
- ⁴M. Hara, T. Wada, T. Fukasawa, and F. Kikuchi, *IEEE Trans. Nucl. Sci.* NS-30 (4), 3639 (1983); R. Hoppe, *Numer. Math.* 36, 389 (1981); W. Wilhelm, *Part. Accel.* 12, 139 (1982).
- ⁵The subject analysis derives from the Laplace equation 3-D analysis of Ref. 6, which is validated in the third dimension by choosing a geometry that calibrates with respect to the second dimension. The second dimension Laplace equation analysis is described in Ref. 7 and validated by experiment in Ref. 8. Also, the 2-D Helmholtz analysis of Ref. 9 derives directly from the analysis of Ref. 7, validated by Ref. 8.
- ⁶J. H. Whealton, R. W. McGaffey, and P. S. Meszaros, *J. Comput. Phys.*, in press; J. H. Whealton, R. W. McGaffey, and P. S. Meszaros, presented at the IEEE International Conference on Plasma Science, San Diego, 1983.
- ⁷J. H. Whealton, *Nucl. Instrum. Methods* 189, 55 (1981); J. H. Whealton, *IEEE Trans. Nucl. Sci.* NS-28, 1358 (1981); J. H. Whealton and J. C. Whitson, *Part. Accel.* 10, 235 (1980); J. H. Whealton, E. F. Jaeger, and J. C. Whitson, *J. Comput. Phys.*, 27, 32 (1978).
- ⁸C. N. Meixner, M. M. Menon, C. C. Tsai, and J. H. Whealton, *J. Appl. Phys.* 52, 1167 (1981); J. H. Whealton, R. W. McGaffey, and W. L. Stirling, *J. Appl. Phys.* 52, 3787 (1981); J. Kim, J. H. Whealton, and G. Schilling, *J. Appl. Phys.* 49, 517 (1978); L. R. Grisham, C. C. Tsai, J. H. Whealton, and W. L. Stirling, *Rev. Sci.*

- Instrum. 48, 1037 (1977); J. H. Whealton, Bull. Am. Phys. Soc. 27, 1136 (1982); J.H. Whealton, L. R. Grisham, C. C. Tsai, and W. L. Stirling, J. Appl. Phys. 49, 3091 (1978); W. L. Gardner et al., Rev. Sci. Instrum. 52, 1625 (1981); J. H. Whealton, R. J. Raridon, R. W. McGaffey, D. H. McCollough, W. L. Stirling, and W. K. Dagenhart, in Proceedings of the Third International Symposium on Production and Neutralization of Negative Ions and Beams (Brookhaven, 1983), pp. 524-532; W. L. Stirling, W. K. Dagenhart, J. J. Donaghy, and J. H. Whealton, in Proceedings of the Third International Symposium on Production and Neutralization of Negative Ions and Beams (Brookhaven, 1983), pp. 450-457; J. H. Whealton, C. C. Tsai, W. K. Dagenhart, W. L. Gardner, H. H. Haselton, J. Kim, M. M. Menon, P. M. Ryan, D. E. Schechter, and W. L. Stirling, Appl. Phys. Lett. 33, 278 (1978).
- ⁹J. H. Whealton, J. W. Wooten, R. W. McGaffey, D. H. McCollough, R. J. Raridon, M. A. Bell, P. S. Meszaros, A. M. Goswitz, and D. J. Hoffman, Bull. Am. Phys. Soc. 28, 1087 (1983).
- ¹⁰J. S. Hornsby, "A Computer Programme for the Solution of Second Order Quasi-Linear Partial Differential Equations of the Elliptic Type Using the Method of Over-Relaxation," CERN-63-7 (European Organization for Nuclear Research, Geneva, 1963).
- ¹¹G. D. Smith, Numerical Solution of Partial Differential Equations: Finite Difference Methods, 2nd ed. (Clarendon Press, Oxford, 1978).
- ¹²R. W. McGaffey, J. H. Whealton, R. J. Raridon, J. W. Wooten, and M. A. Bell, Bull. Am. Phys. Soc. 29, 146 (1984).

INTERNAL DISTRIBUTION

- | | |
|-----------------------|--------------------------------------|
| 1. F. W. Baity | 24. D. J. Strickler |
| 2. K. T. Barry | 25. D. W. Swain |
| 3-4. M. A. Bell | 26. C. C. Tsai |
| 5. R. D. Burris | 27-31. J. H. Whealton |
| 6. B. A. Carreras | 32. T. L. White |
| 7-8. G. L. Chen | 33. J. Sheffield |
| 9-10. D. J. Hoffman | 34-35. Laboratory Records Department |
| 11. J. A. Holmes | 36. Laboratory Records, ORNL-RC |
| 12-13. E. F. Jaeger | 37. Document Reference Section |
| 14. J. F. Lyon | 38. Central Research Library |
| 15-16. R. C. Mann | 39. Fusion Energy Division |
| 17-18. R. W. McGaffey | Library |
| 19. J. K. Munro | 40-41. Fusion Energy Division |
| 20. L. W. Owen | Publications Office |
| 21-22. R. J. Raridon | 42. ORNL Patent Office |
| 23. K. E. Rothe | |

EXTERNAL DISTRIBUTION

43. Office of the Assistant Manager for Energy Research and Development, Department of Energy, Oak Ridge Operations Office, P. O. Box E, Oak Ridge, TN 37831

44. J. D. Callen, Department of Nuclear Engineering, University of Wisconsin, Madison, WI 53706
45. J. F. Clarke, Office of Fusion Energy, Office of Energy Research, ER-50, Germantown, U.S. Department of Energy, Washington, DC 20545
46. R. W. Conn, Department of Chemical, Nuclear, and Thermal Engineering, University of California, Los Angeles, CA 90024
47. S. O. Dean, Director, Fusion Energy Development, Science Applications International Corporation, Gaithersburg, MD 20879
48. H. K. Forsen, Bechtel Group, Inc., Research Engineering, P. O. Box 3965, San Francisco, CA 94105
49. J. R. Gilleland, GA Technologies, Inc., Fusion and Advanced Technology, P.O. Box 81808, San Diego, CA 92138
50. R. W. Gould, Department of Applied Physics, California Institute of Technology, Pasadena, CA 91125
51. R. A. Gross, Plasma Research Library, Columbia University, New York, NY 10027
52. D. M. Meade, Princeton Plasma Physics Laboratory, P.O. Box 451, Princeton, NJ 08544
53. M. Roberts, International Programs, Office of Fusion Energy, Office of Energy Research, ER-52, U.S. Department of Energy, Washington, DC 20545
54. W. M. Stacey, School of Nuclear Engineering and Health Physics, Georgia Institute of Technology, Atlanta, GA 30332
55. D. Steiner, Nuclear Engineering Department, NES Building, Tibbetts Avenue, Rensselaer Polytechnic Institute, Troy, NY 12181

56. R. Varma, Physical Research Laboratory, Navrangpura, Ahmedabad 380009, India
57. Bibliothek, Max-Planck Institut fur Plasmaphysik, D-8046 Garching, Federal Republic of Germany
58. Bibliothek, Institut fur Plasmaphysik, KFA, Postfach 1913, D-5170 Julich, Federal Republic of Germany
59. Bibliotheque, Centre des Recherches en Physique des Plasmas, 21 Avenue des Bains, 1007 Lausanne, Switzerland
60. Bibliotheque, Service du Confinement des Plasmas, CEN/Cadarache, Departement de Recherches sur la Fusion Controlee, 13108 Saint-Paul-lez-Durance, France
61. Documentation S.I.G.N., Departement de la Physique du Plasma et de la Fusion Controlee, Centre d'Etudes Nucleaires, B.P. 85, Centre du Tri, 38041 Grenoble, France
62. Library, Culham Laboratory, UKAEA, Abingdon, Oxfordshire, OX14 3DB, England
63. Library, FOM-Instituut voor Plasma-Fysica, Rijnhuizen, Edisonbaan 14, 3439 MN Nieuwegein, The Netherlands
64. Library, Institute of Plasma Physics, Nagoya University, Nagoya 464, Japan
65. Library, International Centre for Theoretical Physics, Trieste, Italy
66. Library, Laboratorio Gas Ionizzati, CP 56, I-00044 Frascati, Rome, Italy
67. Library, Plasma Physics Laboratory, Kyoto University, Gokasho, Uji, Kyoto, Japan

68. Plasma Research Laboratory, Australian National University,
P.O. Box 4, Canberra, A.C.T. 2000, Australia
69. Thermonuclear Library, Japan Atomic Energy Research Institute,
Tokai-mura, Ibaraki Prefecture, Japan
70. T. V. George, Plasma Technologies Branch, Division of Development
and Technology, Office of Fusion Energy, Office of Energy
Research, ER-531 Germantown, U.S. Department of Energy,
Washington, DC 20545
71. G. M. Haas, Fusion Technologies Branch, Division of Development
and Technology, Office of Fusion Energy, Office of Energy
Research, ER-533 Germantown, U.S. Department of Energy,
Washington, DC 20545
72. E. Oktay, Division of Confinement Systems, Office of Fusion
Energy, Office of Energy Research, ER-55 Germantown,
U.S. Department of Energy, Washington, DC 20545
73. H. S. Staten, Plasma Technologies Branch, Division of Development
and Technology, Office of Fusion Energy, Office of Energy
Research, ER-531 Germantown, U.S. Department of Energy,
Washington, DC 20545
- 74-279. Given distribution as shown in TIC-4500, Magnetic Fusion Energy
Category Distribution UC-20 f.g: Experimental Plasma Physics,
Theoretical Plasma Physics)